Hidden Fine Structure of Quantum Defects Revealed by Single Carbon Nanotube Magneto-Photoluminescence

Younghee Kim, Serguei V. Goupalov, Braden M. Weight, Brendan J. Gifford, Xiaowei He, Avishek Saha, Mijin Kim, Geyou Ao, YuHuang Wang, Ming Zheng, Sergei Tretiak, Stephen K. Doorn,* and Han Htoon*
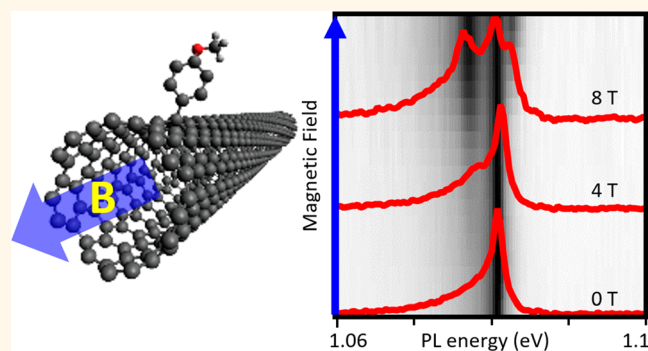
Read Online

ACCESS | Metrics & More | Article Recommendations | SI Supporting Information

ABSTRACT: Organic color-center quantum defects in semiconducting carbon nanotube hosts are rapidly emerging as promising candidates for solid-state quantum information technologies. However, it is unclear whether these defect color-centers could support the spin or pseudospin-dependent excitonic fine structure required for spin manipulation and readout. Here we conducted magneto-photoluminescence spectroscopy on individual organic color-centers and observed the emergence of fine structure states under an 8.5 T magnetic field applied parallel to the nanotube axis. One to five fine structure states emerge depending on the chirality of the nanotube host, nature of chemical functional group, and chemical binding configuration, presenting an exciting opportunity toward developing chemical control of magnetic brightening. We attribute these hidden excitonic fine structure states to field-induced mixing of singlet excitons trapped at sp^3 defects and delocalized band-edge triplet excitons. These findings provide opportunities for using organic color-centers for spintronics, spin-based quantum computing, and quantum sensing.

KEYWORDS: carbon nanotubes, sp^3 defect, magnetic field, photoluminescence, hybridization, triplet

Covalent sp^3 defects of single-walled carbon nanotubes (SWCNTs), often referred to as organic color centers,[1] are rapidly emerging as an important class of materials for defect-driven quantum information technologies.[2−6] These defects, created *via* covalent attachment of various organic functional groups, support spatially localized and optically active exciton states located 130−300 meV below the band-edge transition.[7,8] Due to this deep trapping potential, the trapped exciton can maintain characteristics of a zero dimensional confined system and allow for high purity single photon generation at room temperature (RT).[6,9] Since the trap states are created relative to the band-edge, their emission energies can readily be tuned across the 1.3 to 1.55 μm telecommunication wavelength range *via* attachment of defects on SWCNTs of larger diameters. In addition, solitary sp^3 defect states have recently addressed long-standing challenges that exist in SWCNT applications presented by the diversity and complexity of the band-edge exciton electronic structure.

The electronic structure of semiconducting SWCNTs originates from that of graphene and features a band gap opening at two inequivalent K and K′ valleys of a two-dimensional (2D) Brillouin zone. Enhanced Coulomb interactions due to reduced dimensionality and low dielectric constant lead to strong excitonic effects, whereby excitons can be formed in singlet and triplet spin configurations. As a result, SWCNTs are endowed with a rich series of 16 distinct band-edge exciton states (4 singlets and 12 triplets).[10−12] The optically active odd-parity singlet exciton state is located at an energy higher than the other even-parity singlet and 12 triplet exciton states, all of which have symmetry forbidden optical transitions (dark states). Consequently, the majority of excitons relax to dark states, making the SWCNTs inefficient
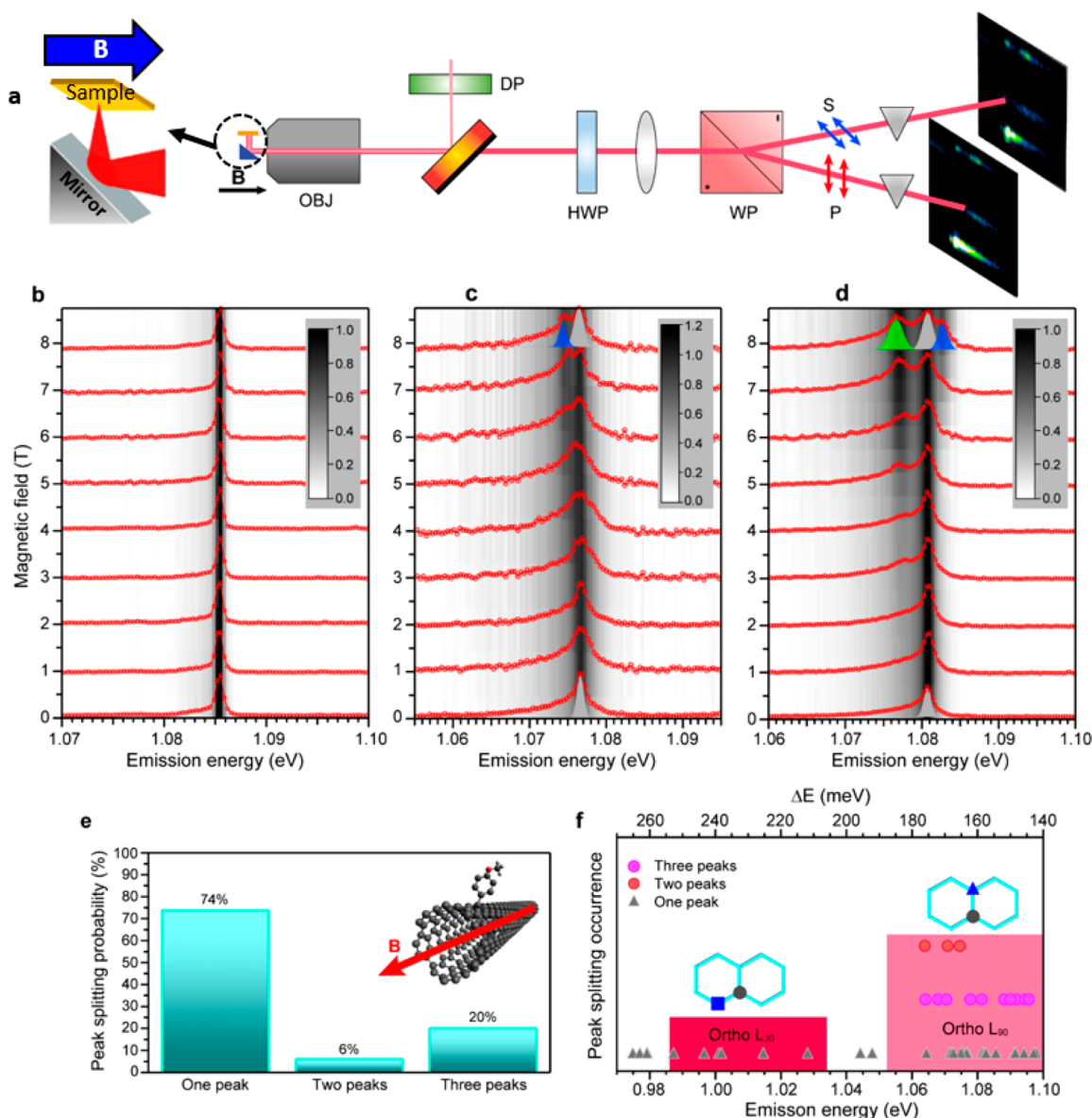
Figure 1. Magnetic brightening of hidden fine structure of localized exciton states (E_{11}^*) in 4-methoxybenzene-functionalized (6,5) SWCNTs. (a) Schematic of the experimental setup. DP: depolarizer, OBJ: objective, HWP: half-wave plate, and WP: Wollaston prism. (b–d) Magneto-photoluminescence spectra of a single defect-state emission in magnetic fields up to 8.5 T, at a fixed temperature (4 K). The single defect state at zero field remained unchanged in (b) or evolved into two or three emissive states in (c) and (d), respectively. The underlying black and white false colored magneto-photoluminescence image, which is normalized to 1, is constructed to demonstrate development of the emissive peak splitting (c,d) or maintaining a consistent single peak (b). (e) Statistics for the observation of one-, two-, and three-peak spectra, based on a total of 50 individual SWCNTs, for which the tube axis is parallel to the magnetic field axis within ±15°. (f) Peak splitting occurrence from 4-methoxybenzene-functionalized (6,5) SWCNTs aligned to the magnetic field vs emission peak energies (bottom) and energy shifts from E_{11} band edge emission (top). Magneto-photoluminescence study reveals that hybridization from spin singlet and triplet quantum states can be found only in ortho L$_{90}$ binding configurations, where the energy level between the two quantum states nearly match.

light emitters with <1% photoluminescence (PL) quantum yield.[11−13] As a result, understanding these dark transitions and harnessing the dark exciton population for a variety of optoelectronic applications have become a major theme in SWCNT research for the past decade.[5,14,15] While an extensive amount of research has been conducted toward understanding and controlling singlet exciton states, only a handful of studies have addressed the properties of the triplet manifold.[13,16,17] Since sp^3 defects are known to trap both bright and dark excitons,[5,7] they allow effective harnessing of the dark excitons and boost the PL quantum yield to ~16% on the ensemble level.[5,14] On the other hand, excitons trapped in the defects are also expected to inherit the complex electronic structure of the band-edge excitons. This excitonic fine structure capable of reflecting spin and valley pseudospin degrees of freedom of trapped excitons has never been investigated, to date. In addition, how the fine structure states of the trapped exciton couple to those of the band-edge excitons also presents an interesting direction to explore.

Due to light carbon atoms in the sp^2 lattice, SWCNTs exhibit a weak spin−orbit interaction (SOI). This, on one hand, could provide desirable long spin coherence, but makes
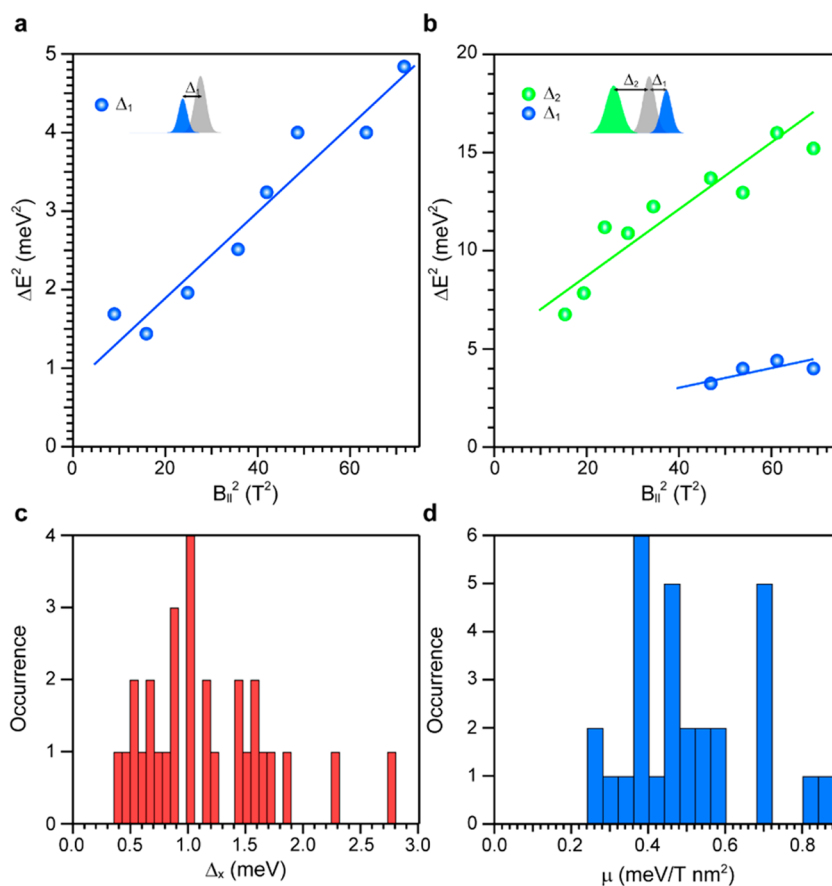
Figure 2. Energy splitting (Δ_x) and coupling constant (μ) and their statistics obtained from the two- and three-peak splitting behaviors of Figure 1c,d. (a,b) Observed experimental excitonic fine structure splitting from two (a) and three (b) emissive quantum states extracted from Figure 1c,d, respectively. $\Delta_1(\Delta_2)$ denotes smaller (bigger) energy splitting from the magnetic-field-induced quantum states with respect to the main PL peak as illustrated by spectra in the insets. The square of the fine structure splitting energies follows a linear dispersion with respect to the square of the magnetic field. The corresponding slopes are ~0.393 meV/T nm². The resultant zero field splitting is ~0.89 meV. In the case of three peak splitting, the strength of the magnetic field dependence on the energy splitting is ~0.376 and ~0.693 meV/T nm² and the zero-field splitting is ~1.01 and ~2.30 meV for Δ_1 and Δ_2, respectively. (c,d) Zero-field splitting energies and coupling constant occurrences extracted from quantum states observed in the magnetic field. Zero-field splitting energies are distributed from ~0.41 to ~2.75 meV and coupling constants range from ~0.25 to ~0.84 meV/T nm².

conventional optical spin manipulation difficult.[18,19] Interestingly, theoretical prediction of impurity-induced spin−orbit coupling[20] and recent reports on colossal enhancement of SOI resulting from conversion of sp^2 to sp^3 bonds in sparsely hydrogenated graphene[21] suggest that the sp^3 defects may also be able to provide a similar enhancement of SOI in SWCNTs. Such enhanced SOI could allow for experimental optical spin manipulation in SWCNTs. Additionally, this could also introduce spin/pseudospin-dependent optical transitions, which could potentially enable entangled photon generation and quantum sensing applications.[22−24]

RESULTS AND DISCUSSION

Emergence of Excitonic Fine Structure under an External Magnetic Field. Aiming to explore these possibilities, we performed low temperature (4 K), single-defect PL spectroscopy studies under 0−8.5 T magnetic field. We investigated hundreds of individual sp^3 defects created on SWCNTs of different chiralities [(6,5) and (11,0)] and functionalized with different chemical functional groups: 4-methoxybenzene, 3,5-dicholoro benzene, $-CH_3$, and divalent-CH_2 (the latter with the dopant carbon atom covalently bound to two adjacent carbon atoms of the nanotube). The

schematics of these functional groups as well as the PL spectra for band-edge and defect emission bands of functionalized SWCNTs are summarized in Figure S1. Figure 1a illustrates the experimental setup. Because the PL of the functionalized SWCNTs is linearly polarized along the tube axis, we used the orientation of linear polarization to determine the angle between the tube axis and the direction of the applied magnetic field (B-field) (See Figure S2). As in the case of the band edge exciton, the magnetic field is found to affect the defect-state PL spectra only when the tube axis aligns nearly parallel to the direction of the B-field.[15,25−27] Figure 1b-d displays three distinct, characteristic magnetic-field-dependent behaviors observed in (6,5) SWCNTs functionalized with 4-methoxybenzene. Out of 121 individual SWCNTs probed, 50 tubes were found with their axes aligned within ±15° of the magnetic field, allowing for evaluation of the B-field effect on individual defect states. PL spectra of 74% of the defect states showed no change with an increase of the magnetic field (see Figure 1b). A behavior similar to the band-edge exciton state, namely the splitting of the defect associated PL peak into two spectral features, with the low-energy peak gaining strength as magnetic field increases, is observed in a small fraction (6%) of the defects (Figure 1c).[25,26] The remaining 20% of the defects
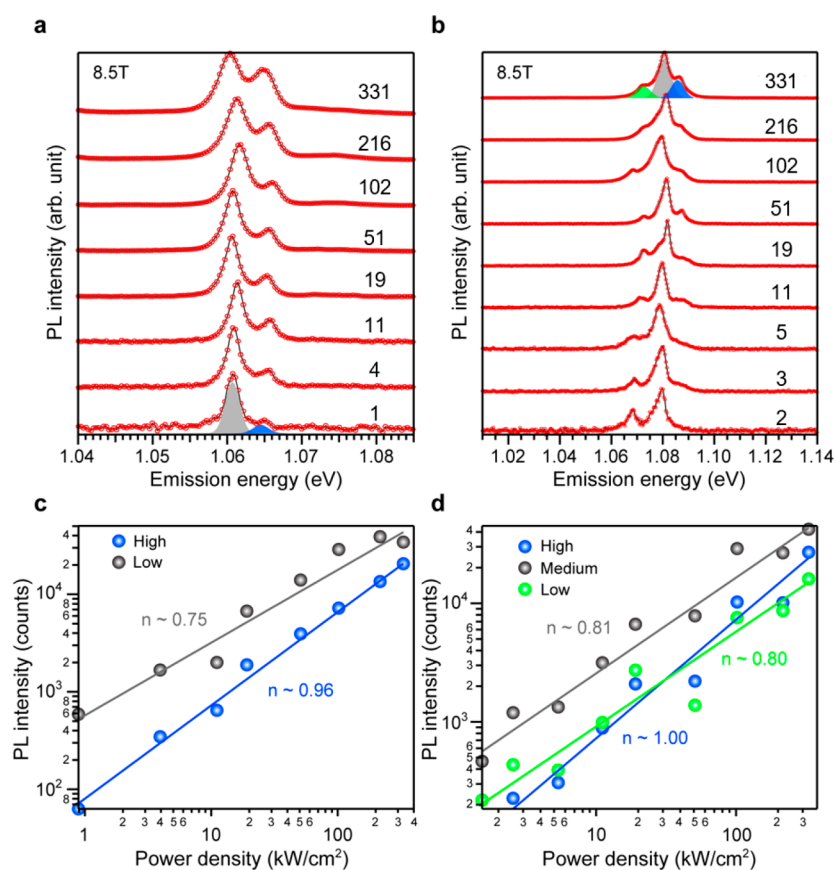
Figure 3. Quantum state intensity dependence on pump power. (a,b) Pump power-dependent spectra for cases of two- (a) and three-peak (b) splitting at the highest magnetic field of 8.5 T. The applied excitation pump powers are indicated on each spectrum with a unit of kW/cm². The examples of peak fitted spectral weights are shown in the colored spectral areas in the lowest pump power in (a) and the highest pump power in (b). (c,d) Log–log plots of PL intensity as a function of the pump power density. The colors of circles match with the colors of the peak fitted areas in (a) and (b). The coefficients of the log–log plots are close to 1, demonstrating that the quantum states induced from the magnetic field originate from exciton fine structure.

display splitting of a single peak into three or more peaks, as shown in Figure 1d and Figure S3 (see Figure 1e for a summary of these statistics). Application of super-resolution analysis (Figure S4) confirms that these peaks originate from a single defect within < ±10 nm accuracy. In both two-peak and three-or-more-peak cases, all the additional peaks are linearly polarized along the tube axis in the same way as the main PL peak at zero field (Figure S5).

Each plot in Figure 1 and Figure S3 illustrates that the relative intensities of low-, medium-, and high-energy defect associated PL peaks, as well as the order in which they emerge with an increase of the magnetic field, vary from one defect to another. Figure 1f shows how defects showing one-, two-, and three-or-more-peak behaviors distribute as a function of their emission energy (lower axis) and energy shift from the E_{11} band edge exciton state (upper axis). Since covalent binding of an aryl group requires capture of a balancing group (−H or −OH) by one of the six nearby carbon atoms, aryl defects can form six distinct chemical configurations, each having distinct trapping potentials.[8] Our previous studies have shown that a diversity of emission energies is found for functionalized (6,5) SWCNTs, with defect-state emission observed in the range 0.918−1.233 eV. These arise primarily from binding configurations in which the captured −H or −OH is located one carbon atom away from the aryl group and oriented at either 30° or 90° from the tube axis, "ortho L_{30}", and "ortho

L_{90}" geometries, respectively (see schematic drawings in the inset of Figure 1f).[6,8] Interestingly, defects exhibiting two- and three-peak splitting were observed only in the spectral range expected for the ortho L_{90} defects, indicating a strong dependence of magnetic brightening behavior on this specific chemical configuration.

Following the analysis employed in the studies devoted to brightening of dark exciton in intrinsic SWCNTs,[25,26] we plot the square of energy splitting for the two-peak and three-peak cases, shown in Figure 1c,d, as a function of the square of B-field strength in Figure 2a,b. While the plot shows linear scaling, extrapolation of the trend reveals that the peaks do not converge to a single peak at zero field, indicating that these peaks emerge as a result of brightening of dark, fine-structure states located in close proximity to the bright states. Relative PL intensities of the brightened states (*i.e.*, PL of brightened peak/PL of the main PL peak) plotted as the function of magnetic field (Figure S6) also display a clear increase of oscillator strength of the brightened states relative to that of the main PL peak. Analysis of the 13 defect states displaying two- and three-peak behavior revealed that the extracted zero-field splitting values vary from 0.41 to 2.75 meV, with the peak of the distribution occurring at ∼1.0 meV (Figure 2c). The coupling constants (μ) extracted from the slope of the $(\Delta E)^2$ *vs* B^2 plot distribute over a range of 0.25−0.84 meV/T nm² (Figure 2d). These μ values fall in the same range as the
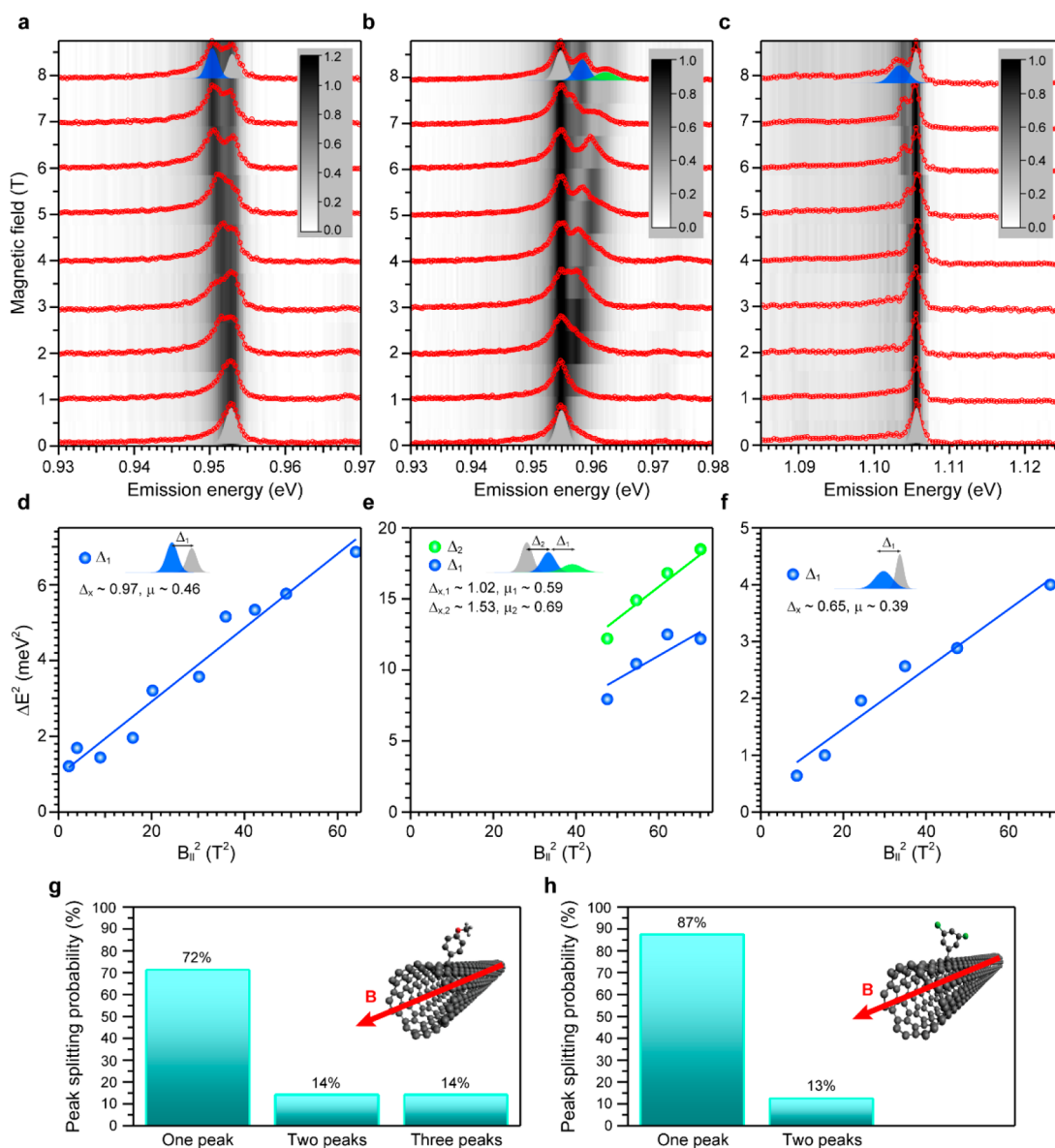
Figure 4. Observed magnetic-field-induced excitonic fine structure from 4-methoxybenzene-functionalized (11,0) and 3,5-dichlorobenzene-functionalized (6,5) SWCNTs. (a−c) Magneto-photoluminescence spectra of defect-state emission from a single 4-methoxybenzene-finctionalized (11,0) SWCNT (a,b) and a single 3,5-dichlorobenzene-functionalized (6,5) SWNCT in (c). The 4-methoxybenzene quantum defect state PL peaks split into two or three emission peaks in the relatively high fields, while the 3,5-dichlorobenzene defect state only splits into two peaks in the highest magnetic field. The normalized 2D images from different types of chemical functionalized SWCNTs clearly demonstrate the gradual side peak evolution at the low- or high-energy side in the magnetic fields. (d−f) Experimental energy splitting of peaks in the magneto-photoluminescence spectra of (a−c). The zero field splitting energies (Δ_x) and the coupling constants (μ) are extracted from the $B_\parallel^2$ *vs* ΔE^2 linear relation. (g,h) Probability of observing the magnetic field induced hybridization with one-, two-, and/or three-peak spectra from a 4-methoxybenzene (g) and 3,5-dichlorobenzene (h) defect, out of 14 and 16 measured tubes, respectively.

proportionality constant for the field-induced Aharonov−Bohm splitting reported for the band-edge excitons.[15,25−27]

To further understand the nature of these brightened PL peaks, we measured PL spectra as a function of laser pump power at 8.5 T applied field (Figure 3a,b). While the pump power-dependent PL spectra show changes in relative PL intensities among the different peaks, log−log plots of PL intensity *vs* pump power (Figure 3c,d) yield a linear relationship with a slope of ~1 (0.75 to 1), indicating that intensities of all the PL peaks scale approximately linearly with the pump power. Notably, PL spectra resulting from quantum cascade recombination of multiexciton states, such as biexciton and three-exciton states, are known to exhibit nonlinear scaling

with pump power (*e.g.*, quadratic scaling with a slope of 2 for biexcitons). Thus, our observation of linear scaling indicates that the brightened PL peaks are not related to these higher order multiexciton states and must originate from the excitonic fine structure.

Influence of SWCNT Chirality, Chemical Functional Groups, And Binding Configurations on Emergence of Excitonic Fine Structure. Finally, to understand how this magnetic brightening behavior varies with the exact nature of the attached chemical functional groups as well as with chirality of the SWCNTs, we investigated defects created (1) on (11,0) SWCNTs by functionalization with 4-methoxybenzene (MeO-Dz) and (2) on (6,5) SWCNTs by functionaliza-

tion with 3,5-dicholorobenzene (Cl$_2$-Dz), methyl (CH$_3$), and methylene (divalent-CH$_2$). In the case of MeO-Dz functionalized (11,0) SWCNTs (Figure 4a,b,d,e), we observed both two- and three-peak splitting behaviors in 14% of the total defects for each case (Figure 4g). More interestingly, while defect emission for (11,0) SWCNTs spreads over the range from 0.947−0.974 eV, both two- and three-peak splitting behaviors were observed only over the 0.947−0.960 eV range, attributable to off-axis ortho L$_{60}$ configurations. On the other hand, for (6,5) SWCNTs functionalized with Cl$_2$-Dz, only three out of 24 Cl$_2$-Dz defects emitting in the ortho L$_{90}$ emission range displayed two-peak splitting, while no three-peak splitting behavior was observed. All CH$_3$ (10) and CH$_2$ (12) functionalized (6,5) tubes show no B-field-dependent splitting (Figure S7), which is consistent with an earlier report on the SWCNT defects of the same functional groups.[28] These results, together with those reported in Figure 1b-d, indicate that the selection of dopant molecular structure, binding configuration, and tube chirality may be further exploited toward controlling the magnetic brightening behavior.

Together, these findings point to the emergence of a magnetic-field-dependent behavior that has never been observed in SWCNTs. Particularly, the appearance of more than two fine-structure features indicates that this phenomenon is different from the brightening of the dark band-edge exciton by an Aharonov−Bohm flux reported in pristine SWCNTs.[15,25−27] Furthermore, observation of the magnetic brightening effect only in a small subset of sp^3 defects emitting in the spectral band assigned to the ortho L$_{90}$ defect geometries and the absence of such behavior in the ortho L$_{30}$ defect-state emission band make the phenomenon more perplexing. A plausible explanation of such behavior involves the energetic alignment of the triplet potential energy surfaces (PES) in the pristine region and the singlet PES in the functionalized region of the SWCNT system (Figure 5). Such alignment, together with an applied external magnetic field, could lead to coupling between the triplet free exciton and defect-bound singlet exciton. The triplet states, as a result, are able to borrow oscillator strength from the defect bound singlet exciton state and participate in PL emission leading to the multipeak features we observed. This coupling would depend critically on the precise energetic alignment of the pristine triplet and localized singlet excitons arising from functionalization. Brightening of the triplet manifold thus would be observed only in a subset of defects meeting this critical requirement. As chemical functional groups and their binding configurations are known to have a strong effect on the defect-state energy,[4,5,8,29] it becomes possible for these factors to directly influence the magnetic brightening behavior as observed experimentally in Figure 4.

Theoretical Models. To support this hypothesis with modeling we use time-dependent density functional theory (TDDFT, see Methods) to calculate energies of singlet and triplet states in both pristine and functionalized SWCNTs. As expected, a good energetic overlap between one of the pristine triplet exciton states and singlet state for an exciton bound to a defect in the ortho L$_{90}$ configuration is observed for (6,5) SWCNT functionalized with monovalent functional groups (i.e., CH$_3$, Cl$_2$-Dz, MeO-Dz) in Figure S8. However, no alignment is observed for the divalent species (i.e., CH$_2$). The calculated energies of the singlet defect states for ortho L$_{30}$ configurations are also observed to be substantially lower than that of the pristine triplets, regardless of differences in
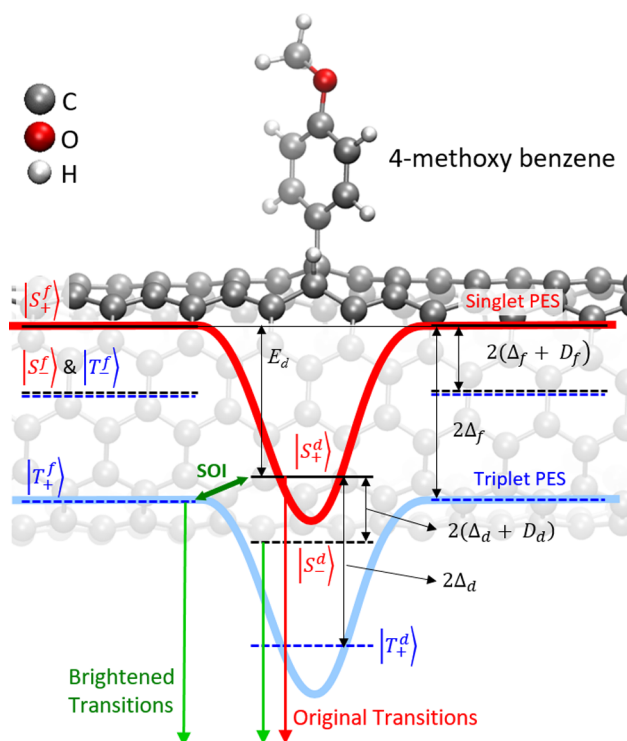

Figure 5. Energy level diagram depicting magnetic field brightening of hidden fine structure. The covalent defect brings the potential energy surface of the singlet state (red line) down to an energy close to that of the free triplet exciton (light blue line). As a result, triplet states can mix with defect singlet states *via* SOI (green double arrow) and can become optically active. Solid and dashed horizontal lines show the bonding and antibonding state of the singlet and triplet direct excitons considered in our four state empirical model (see Methods).

functional groups. These misalignments suggest much weaker coupling between triplet and singlet states and explains the absence of magnetic-field-dependent behaviors reported in Figure 1b and Figure S7. Overall, these computational studies reinforce the plausible description of the emergence of spectral fine structure in the presence of a magnetic field. However, the relative energetics of singlet and triplet states is strongly dependent on the nature of the density functional used and is extremely sensitive to the fraction of the orbital exchange present in the hybrid DFT models.[30] Ultimately, our quantum-chemical simulations lack the sub-10 meV resolution[30] required to quantitatively describe the experimentally observed B-field-dependent behaviors.

To further bolster our qualitative description, we constructed an effective empirical four-state Hamiltonian model. Here, spin-singlet states of direct, defect-bound excitons in the K and K′ valleys ($|S_{KK}^d\rangle$, $|S_{K'K'}^d\rangle$) are coupled to spin-triplet states of free, direct excitons with zero spin projection along SWCNT axis ($|T_{KK}^f\rangle$, $|T_{K'K'}^f\rangle$) *via* Rashba-type SOI arising from broken reflection symmetry about the curved graphene plane of SWCNT[31] (see Methods). While such a curvature-induced SOI has been shown to be too weak to couple singlet and triplet states of free excitons, due to their large energy separation, it could become sufficient to induce coupling and hence brightening when the lowest energy triplet state is close to resonance with the bright defect-bound singlet exciton state (Figure 5). Furthermore, the presence of the defects in our SWCNTs can further enhance the spin−orbit coupling, as it

has been shown that hybridization of the carbon atoms with impurities can lead to a strong enhancement of the SOI in graphene.[20,21]

Using the Hamiltonian described above, we calculated energies and oscillator strengths for its eigenstates, which reduce to the bonding and antibonding combinations of singlet $(|S_{\pm}^{d}\rangle = (|S_{KK}^{d}\rangle \pm |S_{K',K'}^{d}\rangle)/\sqrt{2})$ and triplet $(|T_{\pm}^{f}\rangle = (|T_{KK}^{f}\rangle \pm |T_{K',K'}^{f}\rangle)/\sqrt{2})$ exciton states at zero field and zero spin−orbit coupling. The calculations are performed as a function of external magnetic field for three cases, where the bonding state of a triplet free exciton $(|T_{+}^{f}\rangle)$ and defect-bound singlet exciton state, $|S_{+}^{d}\rangle$, are perfectly aligned in energy (Figure S9a,b) and misaligned by 6 meV (Figure S9c,d) and 12 meV (Figure S9e,f), respectively. Our calculations indeed show that the antibonding state of a defect-bound singlet exciton $|S_{-}^{d}\rangle$, as well as the bonding state of a triplet free exciton, $|T_{+}^{f}\rangle$, can gain significant oscillator strength for perfect alignment and small (6 meV) misalignment cases (Figure S9 a−d).

This simplified model, together with our TDDFT simulations, rationalizes a possible route for emergence of two- and three-peak spectral features that depends on $|T_{+}^{f}\rangle - |S_{+}^{d}\rangle$ energetic alignment, strength of spin−orbit coupling, and $|S_{+}^{d}\rangle - |S_{-}^{d}\rangle$ bright-dark energy splitting for the defect state. For example, when a triplet free exciton, $|T_{+}^{f}\rangle$, and a defect bound singlet exciton state, $|S_{+}^{d}\rangle$, are perfectly aligned in energy, the theoretical prediction in Figure S9a,b can adequately explain the experimental observation of three-peaks in Figure 1d. A more sophisticated theoretical model, however, is necessary to explain all the experimental observations. For example, in addition to four of the 16 possible combinations of free triplet and defect-bound singlet exciton states considered in this model, triplet exciton states with ±1 spin projection as well as indirect excitons are also expected to be in the vicinity of the singlet defect-bound bright exciton. Brightening of these other states could lead to more complex spectral features, such as the five-peak feature illustrated in Figure S3b. Furthermore, while we assume that the defect-bound excitons fully inherit the energy level structure of the band-edge exciton, with the dark $|S_{-}^{d}\rangle$ state residing below the bright $|S_{+}^{d}\rangle$ state, recent studies have revealed some indication that this order could be reversed.[28,32] Such reversal may explain why most defects display a single spectral peak, regardless of magnetic field.

CONCLUSIONS

In conclusion, we report a single tube, low-temperature magneto-photoluminescence spectroscopy study revealing excitonic fine structure of individual sp[3] defects in covalently functionalized SWCNTs. We observed that magnetic brightening of the fine structure varies from one defect to another and manifests only on a subset of SWCNTs. To rationalize these results, we propose coincidental alignment between potential energy surfaces of free triplet excitons and defect-bound singlet excitons as a plausible mechanism. An applied magnetic field then induces coupling between these states, allowing for oscillator strength from the defect state to be shared with the nearby triplet states, which gives rise to the emergence of additional emission peaks. This augments the diversity of tunable electronic features appearing in functionalized SWCNTs by adding capacity for manipulating spin degrees of freedom *via* a magnetic field, which could provide opportunities to explore the poorly understood triplet manifold of SWCNTs. The latter spin states have potential technological

applications ranging from classical and quantum light generation to quantum sensing.

METHODS

Covalent Functionalization of SWCNTs. The (6,5) chirality enriched SWCNTs were isolated from CoMoCAT SG65i (Southwest Nanotechnologies, lot no. SG65i-L39) *via* aqueous two-phase (ATP) extraction[33] or gel chromatography.[29] Samples enriched in the (11,0) chirality were obtained from CoMoCAT EG150X (Southwest Nanotechnologies, lot no. L4) *via* a DNA-based ATP separation.[34] The purified SWCNTs were stabilized in 1 wt/v% sodium dodecyl sulfate (Sigma-Aldrich, >98.5%) for subsequent functionalization. 4-Methoxyaryl and 3,5-dichloroaryl defects were introduced by diazonium reactions.[5,6,14] To create $-CH_3$ and divalent $-CH_2$ defects, we used a previously reported alkylation chemistry.[4] The successful functionalization of SWCNTs was confirmed by the evolution of defect PL peak using a NanoLog spectrofluorometer (HORIBA Jobin Yvon). After the functionalization, the SWCNTs were stabilized by 1 wt/v% sodium deoxycholate (≥97%, Sigma-Aldrich) in aqueous solution.

Single Nanotube Magneto-Photoluminescence Spectroscopy. Magneto-photoluminescence measurements of individual sp[3] defects were performed using a variable-temperature confocal microscope built inside the room-temperature bore of an 8.5T superconducting magnet. To investigate the effect of the magnetic flux threading the nanotube axis, magneto-photoluminescence spectroscopy was carried out under a Voigt geometry, in which the magnetic field is parallel to the sampling surface but is perpendicular to the direction of excitation light propagation. This geometry is achieved by using the specially designed sample holder shown in the inset of Figure 1a. The samples were mounted in a liquid-helium-flow cryostat in a home-built microscope. An infrared 50× objective (Mitutoyo) with N.A. = 0.42 is used to excite the individual SWCNTs with a continuous-wave (CW) Ti-Sapphire laser with an average power density of 2 kW/cm². The wavelength of the laser is tuned to 854 nm to be in resonance with the phonon sideband of the E_{11} band-edge exciton. The laser excitation was depolarized to excite all the SWCNTs regardless of their orientation. The PL image and spectra were acquired with a liquid-nitrogen-cooled InGaAs 2D detector array camera mounted on a 320 mm spectrograph (Princeton). To determine the orientation angle of each SWCNTs with respect to the magnetic field, we measured the linearly polarized emission using a half-wave plate.

Quantum Chemistry Modeling. To calculate singlet and triplet excited state energies, we applied a previously developed quantum chemical methodology for functionalized SWCNTs based on a density functional theory (DFT) and time-dependent DFT (TDDFT) approach.[35,36] Briefly, pristine SWCNTs of (6,5) and (11,0) chiralities were generated with TubeGen software.[37] The caps of the systems were terminated with hydrogen atoms and methylene groups in ratios sufficient to eliminate superfluous midgap states as previously described.[36] The two distinct defect geometries were generated by placing the functional group of interest and a hydrogen atom in either ortho L_{30} or ortho L_{90} positions. The geometries of the resulting structures were optimized using DFT with the range-corrected CAM-B3LYP density functional and STO-3G basis set as implemented by the Gaussian 16 software.[38] Such methodology has been used in the past due to its relative success describing electron localization in functionalized SWCNTs.[35,36] Since emission originates from an excited state, the excited-state geometries were also optimized with TDDFT with the same functional and basis. Subsequently, vertical transition energies for both singlets and triplets were calculated with TDDFT. This procedure was previously applied to both pristine and functionalized SWCNTs successfully.[30,36] Energies acquired from the pristine SWCNTs represent the energetic levels distant from the defect, while energies acquired from the functionalized SWCNTs represent the excited states in the vicinity of the defect.

Effective Empirical Hamiltonian Model. The effective Hamiltonian, written in the basis of states, $|S_{KK}^d\rangle$, $|S_{K'K'}^d\rangle$, $|T_+^f\rangle$, and $|T_{K'K'}^f\rangle$, is

$$H = \begin{bmatrix} \Delta_d + \mu\Phi - E_d & \Delta_d + D_d & 2\lambda_R & 0 \\ \Delta_d + D_d & \Delta_d - \mu\Phi - E_d & -2\lambda_R & -2\lambda_R \\ 2\lambda_R & 0 & \mu\Phi & D_f \\ 0 & -2\lambda_R & D_f & -\mu\Phi \end{bmatrix} \quad (1)$$

where Φ is the magnetic flux threading the cross-section of the nanotube, μ is a coefficient for the Aharonov–Bohm splitting, D describes the spin-independent part of the intervalley coupling, Δ describes the electron–hole exchange interaction (for the microscopic origin of D and Δ for a free exciton, see refs 10 and 39), and λ_R describes the spin–orbit coupling. All these interactions are short-range, and corresponding constants can be different for the defect-bound and free one-dimensional excitons denoted by subscript/superscript d and f, respectively. We assume Δ_d, D_d, and μ to be the same as the values of free excitons and estimate the values of μ to be 0.93 meV/T nm^2 measured for (6,5) nanotubes and $2(\Delta_f + D_f)$ to be ~6 meV based on refs 40−42. E_d is estimated to be ~146 meV from the difference between emission energies of the defect state (~1.094 eV) and the band-edge exciton (E_{11} = 1.24 eV). If we assume that the spin-singlet state of the localized bonding exciton, $|S_+^d\rangle$ is in resonance with the spin-triplet state of the free bonding exciton, $|T_\pm^f\rangle$, then we will have $2\Delta_f = E_d \approx 73$ meV. Using $2(\Delta_f + D_f) \sim 6$ meV, D_f is estimated to be ~ -70 meV. We then assume $D_d = D_f$, and $\Delta_d = \Delta_f$. Rashba-type, spin−orbit coupling, λ_R, originates from a curvature-induced displacement of the p-atomic orbitals forming the π band giving rise to a radial electric field, which circulating electrons experience as a magnetic field proportional to the azimuthal component of their momentum. The strength of this orbit-like coupling is estimated as ~0.3 meV/d (nm) for coupling between free singlet and triplet excitons. In our case, we set this term to a realistic value of 0.5 meV, as it is expected to be enhanced by the presence of defects. The Hamiltonian is diagonalized numerically at a given magnetic field, and the resulting eigenvectors are projected onto the zero-field bonding combination of spin-singlet exciton states in order to find the oscillator strength.

ASSOCIATED CONTENT

Ⓢ Supporting Information

The Supporting Information is available free of charge at https://pubs.acs.org/doi/10.1021/acsnano.9b09548.

> Ensemble PL spectra of 4-methoxybenzene, 3,5-dichlorobenzene, divalent-CH$_2$, and CH$_3$ functionalized SWCNTs, and their schematic of chemical functional groups. Emission intensity modulation through the orientation of linear polarization to determine the emission angle from a SWCNT. Representative three-or-more-peaks in the magnetic field for 4-methoxybenzene defect (6,5) SWCNTs. Super resolution spectroscopic image analysis. Polarization analysis of the newly emerging PL peaks from the magnetic brightening hidden fine structures. Normalized PL peak intensities brightened states in Figure 1c,d plotted as the function of the magnetic field, respectively. Magneto-photoluminescence spectra from single defect states of divalent-CH$_2$ and CH$_3$ functionalized (6,5) SWCNTs. Energy alignment of trapped singlet excion and delocalized triplet exciton manifolds by TDDFT calculation. Numerical calculation results for energies and oscillator strengths for bonding and antibonding states of singlet and triplet exciton states (PDF)

AUTHOR INFORMATION

Corresponding Authors

Stephen K. Doorn − *Center for Integrated Nanotechnologies, Materials Physics and Applications Division, Los Alamos National Laboratory, Los Alamos, New Mexico 87545, United States;* ⓘ orcid.org/0000-0002-9535-2062; Email: skdoorn@lanl.gov

Han Htoon − *Center for Integrated Nanotechnologies, Materials Physics and Applications Division, Los Alamos National Laboratory, Los Alamos, New Mexico 87545, United States;* ⓘ orcid.org/0000-0003-3696-2896; Email: htoon@lanl.gov

Authors

Younghee Kim − *Center for Integrated Nanotechnologies, Materials Physics and Applications Division, Los Alamos National Laboratory, Los Alamos, New Mexico 87545, United States;* ⓘ orcid.org/0000-0002-4499-3783

Serguei V. Goupalov − *Department of Physics, Jackson State University, Jackson, Mississippi 39217, United States; Ioffe Institute, St. Petersburg 194021, Russia;* ⓘ orcid.org/0000-0002-4913-0792

Braden M. Weight − *Department of Physics, North Dakota State University, Fargo, North Dakota 58108, United States;* ⓘ orcid.org/0000-0002-2441-3569

Brendan J. Gifford − *Center for Nonlinear Studies, Theory Division, Los Alamos National Laboratory, Los Alamos, New Mexico 87545, United States;* ⓘ orcid.org/0000-0002-4116-711X

Xiaowei He − *Center for Integrated Nanotechnologies, Materials Physics and Applications Division, Los Alamos National Laboratory, Los Alamos, New Mexico 87545, United States;* ⓘ orcid.org/0000-0002-4982-8250

Avishek Saha − *Center for Integrated Nanotechnologies, Materials Physics and Applications Division, Los Alamos National Laboratory, Los Alamos, New Mexico 87545, United States*

Mijin Kim − *Department of Chemistry and Biochemistry, University of Maryland, College Park, Maryland 20742, United States;* ⓘ orcid.org/0000-0002-7781-9466

Geyou Ao − *Materials Science and Engineering Division, National Institute of Standards and Technology, Gaithersburg, Maryland 20899, United States;* ⓘ orcid.org/0000-0002-9932-3971

YuHuang Wang − *Department of Chemistry and Biochemistry, University of Maryland, College Park, Maryland 20742, United States;* ⓘ orcid.org/0000-0002-5664-1849

Ming Zheng − *Materials Science and Engineering Division, National Institute of Standards and Technology, Gaithersburg, Maryland 20899, United States;* ⓘ orcid.org/0000-0002-8058-1348

Sergei Tretiak − *Center for Integrated Nanotechnologies, Materials Physics and Applications Division and Center for Nonlinear Studies, Theory Division, Los Alamos National Laboratory, Los Alamos, New Mexico 87545, United States;* ⓘ orcid.org/0000-0001-5547-3647

Complete contact information is available at:
https://pubs.acs.org/10.1021/acsnano.9b09548

Author Contributions

H.H. and S.K.D. conceived and designed the experiment. Y.K., under the supervision of H.H. and S.K.D., performed all spectroscopy studies and data analysis. S.V.G. developed effective empirical Hamiltonian model. B.M.W and B.J.G. performed TDDFT simulation under the supervision of S.T. M.K. under the supervision of Y.H.W. synthesized part of the defect-tailored samples. A.G. and M.Z. performed purification

REFERENCES

(1) Srinivasan, K.; Zheng, M. Nanotube Chemistry Tunes Light. *Nat. Photonics* **2017**, *11*, 535.

(2) Brozena, A. H.; Kim, M.; Powell, L. R.; Wang, Y. Controlling the Optical Properties of Carbon Nanotubes with Organic Colour-Centre Quantum Defects. *Nat. Rev. Chem.* **2019**, *3*, 375−392.

(3) Doorn, S. K.; Htoon, H.; Tretiak, S. Photophysics and Quantum Emission Behaviors of Covalently Introduced Defects in Single-Wall Carbon Nanotubes. In *Handbook of Carbon Nanomaterials*, Weisman, R. B., Kono, J., Eds.; World Scientific: Singapore, 2019; Vol. *10*.

(4) Kwon, H.; Furmanchuk, A. o.; Kim, M.; Meany, B.; Guo, Y.; Schatz, G. C.; Wang, Y. Molecularly Tunable Fluorescent Quantum Defects. *J. Am. Chem. Soc.* **2016**, *138*, 6878−6885.

(5) Piao, Y.; Meany, B.; Powell, L. R.; Valley, N.; Kwon, H.; Schatz, G. C.; Wang, Y. Brightening of Carbon Nanotube Photoluminescence through the Incorporation of sp^3 Defects. *Nat. Chem.* **2013**, *5*, 840.

(6) Saha, A.; Gifford, B. J.; He, X.; Ao, G.; Zheng, M.; Kataura, H.; Htoon, H.; Kilina, S.; Tretiak, S.; Doorn, S. K. Narrow-Band Single-Photon Emission through Selective Aryl Functionalization of Zigzag Carbon Nanotubes. *Nat. Chem.* **2018**, *10*, 1089−1095.

(7) Hartmann, N. F.; Velizhanin, K. A.; Haroz, E. H.; Kim, M.; Ma, X.; Wang, Y.; Htoon, H.; Doorn, S. K. Photoluminescence Dynamics of Aryl sp^3 Defect States in Single-Walled Carbon Nanotubes. *ACS Nano* **2016**, *10*, 8355−8365.

(8) He, X.; Gifford, B. J.; Hartmann, N. F.; Ihly, R.; Ma, X.; Kilina, S. V.; Luo, Y.; Shayan, K.; Strauf, S.; Blackburn, J. L.; Tretiak, S.; Doorn, S. K.; Htoon, H. Low-Temperature Single Carbon Nanotube Spectroscopy of sp^3 Quantum Defects. *ACS Nano* **2017**, *11*, 10785−10796.

(9) He, X.; Hartmann, N. F.; Ma, X.; Kim, Y.; Ihly, R.; Blackburn, J. L.; Gao, W.; Kono, J.; Yomogida, Y.; Hirano, A.; Tanaka, T.; Kataura, H.; Htoon, H.; Doorn, S. K. Tunable Room-Temperature Single-Photon Emission at Telecom Wavelengths from sp^3 Defects in Carbon Nanotubes. *Nat. Photonics* **2017**, *11*, 577.

(10) Ando, T. Effects of Valley Mixing and Exchange on Excitons in Carbon Nanotubes with Aharonov-Bohm Flux. *J. Phys. Soc. Jpn.* **2006**, *75*, 024707−024707.

(11) Spataru, C. D.; Ismail-Beigi, S.; Capaz, R. B.; Louie, S. G. Theory and *Ab Initio* Calculation of Radiative Lifetime of Excitons in Semiconducting Carbon Nanotubes. *Phys. Rev. Lett.* **2005**, *95*, 247402.

(12) Perebeinos, V.; Tersoff, J.; Avouris, P. Radiative Lifetime of Excitons in Carbon Nanotubes. *Nano Lett.* **2005**, *5*, 2495−2499.

(13) Stich, D.; Späth, F.; Kraus, H.; Sperlich, A.; Dyakonov, V.; Hertel, T. Triplet-Triplet Exciton Dynamics in Single-Walled Carbon Nanotubes. *Nat. Photonics* **2014**, *8*, 139.

(14) Miyauchi, Y.; Iwamura, M.; Mouri, S.; Kawazoe, T.; Ohtsu, M.; Matsuda, K. Brightening of Excitons in Carbon Nanotubes on Dimensionality Modification. *Nat. Photonics* **2013**, *7*, 715.

(15) Shaver, J.; Kono, J.; Portugall, O.; Krstić, V.; Rikken, G. L. J. A.; Miyauchi, Y.; Maruyama, S.; Perebeinos, V. Magnetic Brightening of Carbon Nanotube Photoluminescence Through Symmetry Breaking. *Nano Lett.* **2007**, *7*, 1851−1855.

(16) Mohite, A. D.; Santos, T. S.; Moodera, J. S.; Alphenaar, B. W. Observation of the Triplet Exciton in EuS-Coated Single-Walled Nanotubes. *Nat. Nanotechnol.* **2009**, *4*, 425.

(17) Nagatsu, K.; Chiashi, S.; Konabe, S.; Homma, Y. Brightening of Triplet Dark Excitons by Atomic Hydrogen Adsorption in Single-Walled Carbon Nanotubes Observed by Photoluminescence Spectroscopy. *Phys. Rev. Lett.* **2010**, *105*, 157403.

(18) Galland, C.; Imamoğlu, A. All-Optical Manipulation of Electron Spins in Carbon-Nanotube Quantum Dots. *Phys. Rev. Lett.* **2008**, *101*, 157404.

(19) Pályi, A.; Struck, P. R.; Rudner, M.; Flensberg, K.; Burkard, G. Spin-Orbit-Induced Strong Coupling of a Single Spin to a Nanomechanical Resonator. *Phys. Rev. Lett.* **2012**, *108*, 206811.

(20) Castro Neto, A. H.; Guinea, F. Impurity-Induced Spin-Orbit Coupling in Graphene. *Phys. Rev. Lett.* **2009**, *103*, 026804.

(21) Balakrishnan, J.; Kok Wai Koon, G.; Jaiswal, M.; Castro Neto, A. H.; Özyilmaz, B. Colossal Enhancement of Spin-Orbit Coupling in Weakly Hydrogenated Graphene. *Nat. Phys.* **2013**, *9*, 284.

(22) Saha, A.; Gifford, B. J.; He, X.; Ao, G.; Zheng, M.; Kataura, H.; Htoon, H.; Kilina, S.; Tretiak, S.; Doorn, S. K. Narrow-Band Single-Photon Emission Through Selective Aryl Functionalization of Zigzag Carbon Nanotubes. *Nat. Chem.* **2018**, *10*, 1089.

(23) Awschalom, D. D.; Hanson, R.; Wrachtrup, J.; Zhou, B. B. Quantum Technologies with Optically Interfaced Solid-State Spins. *Nat. Photonics* **2018**, *12*, 516−527.

(24) Atatüre, M.; Englund, D.; Vamivakas, N.; Lee, S.-Y.; Wrachtrup, J. Material Platforms for Spin-Based Photonic Quantum Technologies. *Nat. Rev. Mater.* **2018**, *3*, 38−51.

(25) Srivastava, A.; Htoon, H.; Klimov, V. I.; Kono, J. Direct Observation of Dark Excitons in Individual Carbon Nanotubes: Inhomogeneity in the Exchange Splitting. *Phys. Rev. Lett.* **2008**, *101*, 087402.

(26) Matsunaga, R.; Matsuda, K.; Kanemitsu, Y. Evidence for Dark Excitons in a Single Carbon Nanotube Due To the Aharonov-Bohm Defect. *Phys. Rev. Lett.* **2008**, *101*, 147404.

(27) Mortimer, I. B.; Nicholas, R. J. Role of Bright and Dark Excitons in the Temperature-Dependent Photoluminescence of Carbon Nanotubes. *Phys. Rev. Lett.* **2007**, *98*, 027404.

(28) Kwon, H.; Kim, M.; Nutz, M.; Hartmann, N. F.; Perrin, V.; Meany, B.; Hofmann, M. S.; Clark, C. W.; Htoon, H.; Doorn, S. K.; Högele, A.; Wang, Y. Probing Trions at Chemically Tailored Trapping Defects. *ACS Cent. Sci.* **2019**, *5*, 1786−1794.

(29) Kim, M.; Wu, X.; Ao, G.; He, X.; Kwon, H.; Hartmann, N. F.; Zheng, M.; Doorn, S. K.; Wang, Y. Mapping Structure-Property Relationships of Organic Color Centers. *Chem.* **2018**, *4*, 2180−2191.

(30) Tretiak, S. Triplet State Absorption in Carbon Nanotubes: A TD-DFT Study. *Nano Lett.* **2007**, *7*, 2201−2206.

(31) Kuemmeth, F.; Ilani, S.; Ralph, D. C.; McEuen, P. L. Coupling of Spin and Orbital Motion of Electrons in Carbon Nanotubes. *Nature* **2008**, *452*, 448.

(32) Kim, M.; Adamska, L.; Hartmann, N. F.; Kwon, H.; Liu, J.; Velizhanin, K. A.; Piao, Y.; Powell, L. R.; Meany, B.; Doorn, S. K.; Tretiak, S.; Wang, Y. Fluorescent Carbon Nanotube Defects Manifest Substantial Vibrational Reorganization. *J. Phys. Chem. C* **2016**, *120*, 11268−11276.

(33) Subbaiyan, N. K.; Cambré, S.; Parra-Vasquez, A. N. G.; Hároz, E. H.; Doorn, S. K.; Duque, J. G. Role of Surfactants and Salt in Aqueous Two-Phase Separation of Carbon Nanotubes toward Simple Chirality Isolation. *ACS Nano* **2014**, *8*, 1619−1628.

(34) Ao, G.; Streit, J. K.; Fagan, J. A.; Zheng, M. Differentiating Left- and Right-Handed Carbon Nanotubes by DNA. *J. Am. Chem. Soc.* **2016**, *138*, 16677−16685.

(35) Adamska, L.; Nazin, G. V.; Doorn, S. K.; Tretiak, S. Self-Trapping of Charge Carriers in Semiconducting Carbon Nanotubes: Structural Analysis. *J. Phys. Chem. Lett.* **2015**, *6*, 3873−3879.

(36) Gifford, B. J.; Sifain, A. E.; Htoon, H.; Doorn, S. K.; Kilina, S.; Tretiak, S. Correction Scheme for Comparison of Computed and Experimental Optical Transition Energies in Functionalized Single-Walled Carbon Nanotubes. *J. Phys. Chem. Lett.* **2018**, *9*, 2460−2468.

(37) Frey, J. T.; Doren, D. J. *Tube Gen 3.4*; University of Delaware: Newark, DE, 2011.

(38) Frisch, M. J.; Trucks, G. W.; Schlegel, H. B.; Scuseria, G. E.; Robb, M. A.; Cheeseman, J. R.; Scalmani, G.; Barone, V.; Mennucci, B.; Petersson, G. A.; Nakatsuji, H.; Caricato, M.; Li, X.; Hratchian, H. P.; Izmaylov, A. F.; Bloino, J.; Zheng, G.; Sonnenberg, J. L.; Hada, M.; Ehara, M.; Toyota, K.; Fukuda, R.; Hasegawa, J.; Ishida, M.; Nakajima, T.; Honda, Y.; Kitao, O.; Nakai, H.; Vreven, T.; Montgomery, J. A., Jr.; Peralta, J. E.; Ogliaro, F.; Bearpark, M.; Heyd, J. J.; Brothers, E.; Kudin, K. N.; Staroverov, V. N.; Kobayashi, R.; Normand, J.; Raghavachari, K.; Rendell, A.; Burant, J. C.; Iyengar, S. S.; Tomasi, J.; Cossi, M.; Rega, N.; Millam, J. M.; Klene, M.; Knox, J. E.; Cross, J. B.; Bakken, V.; Adamo, C.; Jaramillo, J.; Gomperts, R.; Stratmann, R. E.; Yazyev, O.; Austin, A. J.; Cammi, R.; Pomelli, C.; Ochterski, J. W.; Martin, R. L.; Morokuma, K.; Zakrzewski, V. G.; Voth, G. A.; Salvador, P.; Dannenberg, J. J.; Dapprich, S.; Daniels, A. D.; Farkas, O.; Foresman, J. B.; Ortiz, J. V.; Cioslowski, J.; Fox, D. J. *Gaussian 16*, Rev. C.01; Gaussian, Inc.: Wallingford, CT, 2016.

(39) Goupalov, S. V. Excitons in Semiconductor Carbon Nanotubes: A Momentum-Space Perspective. *Chem. Phys.* **2013**, *413*, 20−28.

(40) Shaver, J.; Crooker, S. A.; Fagan, J. A.; Hobbie, E. K.; Ubrig, N.; Portugall, O.; Perebeinos, V.; Avouris, P.; Kono, J. Magneto-Optical Spectroscopy of Highly Aligned Carbon Nanotubes: Identifying the Role of Threading Magnetic Flux. *Phys. Rev. B: Condens. Matter Mater. Phys.* **2008**, *78*, 081402.

(41) Luo, L.; Chatzakis, I.; Patz, A.; Wang, J. Ultrafast Terahertz Probes of Interacting Dark Excitons in Chirality-Specific Semiconducting Single-Walled Carbon Nanotubes. *Phys. Rev. Lett.* **2015**, *114*, 107402.

(42) Zhou, W.; Sasaki, T.; Nakamura, D.; Liu, H.; Kataura, H.; Takeyama, S. Band-Edge Exciton States in a Single-Walled Carbon Nanotube Revealed by Magneto-Optical Spectroscopy in Ultrahigh Magnetic Fields. *Phys. Rev. B: Condens. Matter Mater. Phys.* **2013**, *87*, 241406.